Journal of Materials Chemistry C

Accepted Manuscript

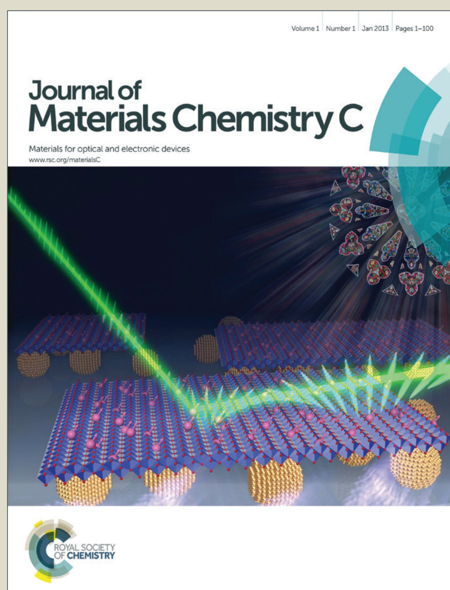

This is an *Accepted Manuscript*, which has been through the Royal Society of Chemistry peer review process and has been accepted for publication.

Accepted Manuscripts are published online shortly after acceptance, before technical editing, formatting and proof reading. Using this free service, authors can make their results available to the community, in citable form, before we publish the edited article. We will replace this *Accepted Manuscript* with the edited and formatted *Advance Article* as soon as it is available.

You can find more information about *Accepted Manuscripts* in the Information for Authors.

Please note that technical editing may introduce minor changes to the text and/or graphics, which may alter content. The journal's standard Terms & Conditions and the Ethical guidelines still apply. In no event shall the Royal Society of Chemistry be held responsible for any errors or omissions in this *Accepted Manuscript* or any consequences arising from the use of any information it contains.

ROYAL SOCIETY OF CHEMISTRY

www.rsc.org/materialsC

Journal of Materials Chemistry C Accepted Manuscript

High thermoelectric performance of a defect α-In_2Se_3-based solid solution upon Zn substitution for In

Jiaolin Cui[1 *], Li Wang[1,2], Zhengliang Du[1], Pengzhan Ying[2], Yuan Deng[3 *]

Received (in XXX, XXX) Xth XXXXXXXXX 200X, Accepted Xth XXXXXXXXX 200X
DOI: 10.1039/b000000x

ABSTRACT In this project, we have successfully manipulated the lattice defects in α-In_2Se_3-based solid solutions ($In_{2-x}Zn_xSe_3$) upon proper substitutions of Zn for In, via a non-equilibrium fabrication technology of materials (NEFT). The manipulation of the defects centers on reducing the number of interstitial In atoms (In_i) and Se vacancies (V_{Se}), and creating a new antisite defect Zn_{In} as a donor. By such means, the lattice structure tends to be ordering, and also more stabilized than that of pure α-In_2Se_3. At the meantime, the carrier concentration (n) and mobility (μ) have increased by 1~2 orders of magnitude. As a consequence, the solid solution at x=0.01 gives the highest TE figure of merit (ZT) of 1.23(±0.22) in the pressing direction at 916K, which is about 4.7 times that of virgin α-In_2Se_3 (ZT=0.26). This achieved TE performance is mainly due to the remarkable improvement of the electrical conductivity that increases from 0.53×10^3 ($\Omega^{-1}m^{-1}$) at x=0 to 4.88×10^3 ($\Omega^{-1}m^{-1}$) at x=0.01 at 916K, in spite of the enhancement of the lattice thermal conductivity (κ_L) from 0.26 ($wm^{-1}k^{-1}$) to 0.32 ($wm^{-1}k^{-1}$).

1. Introduction

The efficiency of thermoelectric (TE) devices largely depends on the dimensionless figure of merit (ZT) of the materials, which is defined as $ZT=(\alpha^2\sigma/\kappa)T$, where α, σ and κ are each the Seebeck coefficient, electrical conductivity and total thermal conductivity. The total κ mainly consists of electronic (κ_e) and lattice (κ_L) components. As to the layered semiconductors that have relatively wide bandgaps, the main challenge is to improve their electrical conductivities while simultaneously maintain high Seebeck coefficients.

Although a remarkable improvement in TE performance has been made in recent decades, achieved either by nanostructuring,[1] band structure engineering,[2] or thermopower waves based energy sources, which result in exceptionally high voltage output and specific power,[3] there still remains necessity to explore new materials, especially wide gap semiconductors, that are potentially competent TE candidates.

Pure α-In_2Se_3 is one of the typical wide gap semiconductor (E_g=1.42eV) with a layered structure (space group $P6_3$/mmc (hexagonal) and R-3m (rhombohedral)).[4,5] It is difficult to synthesize single phase, as its phase transformations are rather complicated.[5] Although doping of impurities, such as Ag, Cu, Mg, Cd, Bi, Sb and I, could not change its n-type conduction,[6] the noble metals like Cu and Ag do not substitute easily in In–Se but are prone to forming other Cu/Ag-containing compounds, such as $(In_2Se_3)_{9.91}(Cu_2Se)_{0.09}$ or In_5AgSe_8, rather than pure α(2H)-In_2Se_3.[7,8] That is why we are not able to manage and control the TE performance of the α-In_2Se_3 up till now.[7]

Besides, α-In_2Se_3 is a semiconductor with many defects. The whole structure of α-In_2Se_3 is arranged in slabs with two layers per unit cell along the c-axis. Each layer is formed in pockets of two In and three Se sub-layers in the sequence of Se-In-Se-In-Se. The bonding between In and Se is strongly covalent, while the interlayer interaction (Se-Se) is of weak van der Waals (VDW) type,[5(b),9] which represents one-third of empty indium sites.[4,9] The VDW gap, which is one of the defects in α-In_2Se_3, is similar to what we have observed in other layered compounds like Bi_2Te_3- or In_4Se_3.[10]

In addition to VDW gap in α-In_2Se_3, there are other kinds of defects. The stoichiometric vacancies in the cationic sites acting as donor centres are treated as defects supporting the exchange of their positions with In cations.[11] Such exchange is speculated to be the origin of free carriers.[12] The positioning of In in the lattice is still a rather puzzling problem. One part of In atoms occupy the normal cationic sites instead of stoichiometric vacant positions, while the other excess part might act as interstitial ones.[12] The excess of In could be considered as a lack of Se. Therefore, there are at least four kinds of defects in the virgin α-In_2Se_3, that is, VDW gap, cationic vacancy V_{In}, interstitial In atom (In_i) and anionic vacancy Se (V_{Se}). If we are able to manipulate these large numbers of intrinsic defects, it is anticipated that both the electrical and thermal conductivities of materials can be tailored.

In this work, we try to continue to tune the TE transport properties by manipulating such defects using following strategies: (1) attempting to decrease the concentration of interstitial In atoms (In_i) (or Se vacancies, V_{Se}) to encourage positional interchanges between the vacancies and cations themselves, by which means we are able to enhance the hole mobility and concentration;[12,13] (2) incorporation of impurity into the cationic sublattice to create new active defects that will increase the lattice distortion, and thereby increase the high frequency phonon scattering. These two strategies are expected to be applied in a synergistic manner.

The above-noted strategies are realized by substitution of Zn for In in α-In_2Se_3, along with the application of non-equilibrium fabrication technology of materials (NEFT). We select element Zn as a substituting atom because the element Zn has a relatively low electronegativity (1.65) and small atomic radius, hence it can easily occupy the cationic or interstitial sites using NEFT. As such, we attain the highest ZT value of 1.23(±0.22) at 916K through remarkably improving electrical conductivity by enhancing the carrier concentration (n) and mobility (μ).

2. Experimental

Sample preparations Based on the previous experiments on Cu/Ag incorporated In_2Se_3,[7] the solubility of metallic element Zn in In_2Se_3 might also be limited. Therefore, we have introduced just a small amount of Zn to In_2Se_3 in this project, and employed a non-equilibrium fabrication technology (NEFT) to prepare the materials. The detailed procedures of NEFT are described below: The mixtures, which were prepared according to $In_{2-x}Zn_xSe_3$ (x=0, 0.005, 0.01, 0.015, 0.02), were melted at 1373K for 24h in vacuum, and then rapidly quenched in ice water to room temperature (RT). The rapid cooling procedure is very necessary as it can avoid the formations of β- and/or γ-In_2Se_3[14] and defect annihilation[12(a)], and also especially, it could lead Zn atoms to enter the interstitial sites. The as-solidified ingots were pulverized and then ball milled at a rotation rate of 350 rpm for 10h in stainless steel bowls that contain benzinum. Subsequently, the dried powders were sintered by using spark plasma sintering apparatus (SPS-1030) under a pressure of 55 MPa and at the highest temperature of 923K. The total sintering time is less than 2min, which includes 20 seconds of holding time, 10s each at around 470 K and 923K respectively. The purpose of such a rapid sintering technology is to avoid the annealing effect caused by the interdiffusion of elements, and to fix the incorporated Zn atoms in the lattices at the same time.

The densities of the sintered samples, which are about 95% theoretical ones, were measured by using Archimedes' method. Each sample was cut into ~3 mm slices measuring ~2.5 mm × 13 mm out of the sintered block, whose size is ϕ20 mm × 2.5 mm, for electrical property measurements.

Structural and chemical composition analyses The structural analysis of the powders was made by powder X-ray diffractometer (D8 Advance) operating at 50 kV and 40 mA. Cu Ka radiation (λ=0.15406 nm) and a scan rate of 4° min^{-1} were used to record the patterns ranging from 10° to 140°. The chemical compositions were determined by an electron probe micro-analyzer (EPMA) (S-4800, Hitachi, Japan) with accuracy > 97%.

X-ray photoelectron spectroscopy (XPS) measurements were performed on an AXIS ULTRA DLD equipped with a monochromatic Al Kα X-ray source (30 mA, 15 kV) and a hybrid lens. Samples were sputter-cleaned with an Ar^+ ion beam until the core-line peaks associated with surface oxides were no longer observed in the XPS spectra. High-resolution core-line spectra of $Zn2p_{3/2}$, $In3d_{5/2}$, and $Se3d_{7/2}$ were collected. In this work, four samples of $In_{2-x}Zn_xSe_3$ (x=0,0.005,0.01,0.02) were examined, and pure In_2Se_3 was examined for comparison.

Raman spectra of three powdered $In_{2-x}Zn_xSe_3$ samples (x=0,0.005,0.01) were recorded at 300 K from 50 to 4000 cm^{-1} at 0.6 cm^{-1} resolution using an Invia-Reflex Raman spectrometer with Nd:YAG laser source (l= 532.0 nm). A 50×objective lens was employed via a confocal geometry to transmit the incident laser beam and collect the scattered radiation. Laser intensity was mandatorily attenuated to prevent decomposing the samples.

When calculating the formation energies, we used the generalized gradient approximation (GGA), a cutoff energy of 400 eV and a k mesh of 4 × 4 × 3. The other calculation procedure was reported in *ref.*15.

TE transport property measurements The Hall coefficient (R_h) measurements at RT were conducted on a Physical Property Measurement System (PPMS, Model-9) using a four probe configuration with a magnetic field sweeping between ±1.5 T, and were performed on rectangular samples with size 2 × 2 × 8 cm^3. The Hall mobilities (μ) and carrier concentrations (n) were subsequently calculated based on the relations $\mu = -R_h\sigma$ and $n = -1/(eR_h)$ respectively, where e is the electron charge. The current and Hall voltage leads were fine copper wires, and the contacts were made of silver paste.

The Seebeck coefficients (α) and electrical conductivities (σ) were measured as a function of temperature using ULVAC ZEM-2, 3 instrument systems in a helium atmosphere between RT and 916K. A temperature difference of approximately 5°C was applied between the two terminals of the sample in order to measure the Seebeck coefficient, whereas the electrical conductivity was measured using the four-probe method. The measurement uncertainties are: 6% for electrical conductivity, 5% for Seebeck coefficient. The thermal conductivities (κ) at RT~916 K were calculated as the product of the material densities, specific heats and thermal diffusivities (with uncertainty below 10%) measured using TC-1200RH. The total uncertainty for ZT is 18%. The lattice contributions (κ_L) were obtained by subtracting the electronic part (κ_e) from the total κ, i.e., $\kappa_L=\kappa-\kappa_e$. Here κ_e is expressed by the Wiedemann–Franz law, $\kappa_e = L_0\sigma T$, where L_0 is the Lorenz number, estimated at 2.45×10^{-8} $W\Omega K^{-2}$. The parameters were finalized after several repeated measurements using different samples.

3. Results and discussions

3.1 Compositional and structural analyses

The differential thermal analysis (DTA) data confirms that there is no phase transformation below 973 K (see Supplementary Figure 1). Such a result might be due to the fact that the phase transformation needs long incubation time for nucleation and relatively high temperature for growth.[9]

The chemical compositions for $In_{2-x}Zn_xSe_3$ each taken from a mapping of EPMA are shown in Supplementary Table 1, and a mapping picture of $In_{2-x}Zn_xSe_3$ (x=0.01) is demonstrated in the Supplementary Figure 2. In Supplementary Table 1 we have observed what we expected a little deficiency in Se and an excess in In. In addition, the molars of In, Zn and Se identified are close to those of as-prepared materials, suggesting that the Zn composition is almost as intended as the final samples.

The XRD analysis shows that materials exhibit α-In_2Se_3-based solid solution (space group: *P63*/*mmc*, PDF:34-1279) until x=0.015 (see Fig.1a), while a minor impurity phase $Zn_{0.4}In_2Se_{3.4}$ was identified at $x\geq0.015$.

In order to confirm the incorporation of Zn into the crystal lattice, we have determined the oxidation states of Zn, In and Se using XPS spectra of Zn2p, In3d and Se3d in $In_{2-x}Zn_xSe_3$ (see Supplementary Figure 3). The binding energy (BE) values for x=0.01 with uncertainties estimated at ~±0.01 eV are listed in Supplementary Table 2, where we observed that the BE value of $Zn2p_{3/2}$ (1021.80eV) is higher than that of single element Zn (1021.45eV), but very close to that of ZnTe.[16] We therefore confirm the existence of ionic Zn^{2+}. The $In3d_{5/2}$ BE (444.70eV) is higher than that of elemental In (443.80eV), but almost equal to those in In_2Se_3 (444.60eV) and In_2O_3 (444.70eV),[16] which indicates the presence of positively charged In^{3+} species. The $Se3d_{7/2}$ BE (54.30eV) analyzed is very close to that of Bi_2Se_3 (54.20eV), confirming the presence of Se^{2-}. We have therefore verified the incorporation of Zn into the crystal lattice.

However, the occupation of Zn in the crystal lattice needs further confirmation. Therefore, we have calculated the formation energies (E_f), which are 1.89 eV, 10.52 eV or -1.67 eV each, when Zn occupies the In lattice, Se lattice or interstitial sites. In terms of the E_f data, we confirm that Zn should preferentially occupy the interstitial sites, and are least likely to occupy Se lattice. However, it is still possible to occupy In cation sites. Nevertheless, the occupation of Zn in the van der Waals (VDW) gaps should be ruled out, because no remarkable elongation of

Journal of Materials Chemistry C Accepted Manuscript

This journal is © The Royal Society of Chemistry [year]

the lattice constant c (see Fig. 1b)[5(a), 12(a), 17] has been observed, neither were visible diffraction peaks observed below 15° based on small angle X-ray diffraction analyses (see Supplementary Figure 4). Based on the above compositional and elemental incorporations, we believe that the number of both the interstitial In (In_i) and Se vacancies (V_{Se}) should be reduced, and the antisite defect Zn_{In} is expected to be created.

3.2 TE transport properties

The electrical properties (α and σ) against temperature (T) have been measured along ($C_{//}$) and perpendicular to ($C\perp$) the pressing directions. The results ($C_{//}$) are shown in Fig.2. Generally, the absolute Seebeck coefficient ($|\alpha|$) gets small as Zn content increases, except for the sample at x=0.02, which gives a little higher $|\alpha|$ values than those at x=0.01. This phenomenon is attributed to the boundary resistances of heat and electricity[18] caused by the precipitation of the impurity phase $Zn_{0.4}In_2Se_{3.4}$, which thereby brings in the boundary Seebeck coefficient. Apart from that, the maximum Seebeck coefficient seems to shift to the higher temperature side as Zn content increases. For example, the maximum $|\alpha|$ value at x=0 appears at ~700K, while those at x=0.01 and 0.02 around 480K and 560K, respectively. However, the Seebeck coefficients for different materials gradually approach the same value as T elevates to 916K (see Fig.2a). The electrical conductivities (σ) increases with temperature increasing, revealing semiconducting behaviour. The σ values also increases with x increasing, except for the sample at x=0.02. It seems that the boundary resistances should also influence the electrical conductivities, as the σ values at x=0.02 are lower than those at x=0.01 (see Fig.2b). The sample at x=0.01 gives the highest σ value 4.88×10^3 ($\Omega^{-1}m^{-1}$) at 916K, while the virgin α-In_2Se_3 gives only 0.53×10^3 ($\Omega^{-1}m^{-1}$).

The lattice thermal conductivity (κ_L), shown in Fig.2c, takes more than 70% of total κ (see Supplementary Figure 5), indicating that the phonon scattering mechanism dominates over all the temperature range. Besides, the temperature dependences of κ_L in the Zn-containing $In_{2-x}Zn_xSe_3$ are different from that of pure α-In_2Se_3, with the κ_L in the former enhancing mildly with the temperature up to 815K, and then reducing, whereas that in the latter reduces with the temperature increasing across the all temperature range. Above ~700K, the Zn-containing $In_{2-x}Zn_xSe_3$ has higher κ_L values than in the case of pure α-In_2Se_3, indicating reduced phonon scattering caused by diminished lattice distortion. The κ_L (κ) values of the sample $In_{2-x}Zn_xSe_3$ (x=0.01) are 0.26wm^{-1}k^{-1} and 0.37(wm^{-1}k^{-1}) at 916K respectively, which enhance by a factor of 1.24 and 1.68 compared to those of pure α-In_2Se_3, as shown in Fig.2(c) and Supplementary Figure 5.

Combining the above three physical parameters (α, σ and κ), we have attained the TE figure of merit (ZT) (Fig.2d) as a function of temperature, which increases with temperature increasing for all samples. The highest ZT value is 1.23 (±0.22) at 916K for x=0.01, which is about 4.7 times that of pure α-In_2Se_3. This material can be comparable to the state-of-the-art semiconductors with chalcopyrite structures, like CuIn(Ga)Te_2[19] and $AgInSe_2$-based materials,[15(b)] and can also be comparable to other layered TE materials, like Bi_2Te_3 or In_4Se_3 based-semiconductors.[20,21] It shows a promising future for applications in the relatively high temperatures.

The TE properties of $In_{2-x}Zn_xSe_3$ (x=0~0.02) perpendicular to the pressing direction ($C\perp$) are shown in Fig. 3. Similarly, the peak $|\alpha|$ value, as what is shown in the case of in $C_{//}$, gets small as Zn content increases, while the sample at x=0.02 gives the highest due to the precipitation of the impurity phase $Zn_{0.4}In_2Se_{3.4}$. The $|\alpha|$ values for four samples gradually approach at 916K (Fig.3a). The sample at x=0.01 in $C\perp$ gives the highest σ value of 5.13×10^3 ($\Omega^{-1}m^{-1}$) at 916K, while the pure α-In_2Se_3 gives only 0.92×10^3 ($\Omega^{-1}m^{-1}$) (Fig.3b). Besides, σ values roughly increases with temperature increasing, also exhibiting the semiconducting behaviour. The electrical conductivities (σ) for all the samples in ($C\perp$) are higher than those in $C_{//}$.

The κ_L (κ) values of Zn-containing $In_{2-x}Zn_xSe_3$ in $C\perp$, which are 0.42 (0.53wm^{-1}k^{-1}) at 916K, are higher than those in $C_{//}$. Besides, both sets of κ_L (κ) values (in $C_{//}$ and $C\perp$) shows similar compositional dependence (Fig.2c, 3c and Supplementary Figure 5, 6). The highest ZT value in $C\perp$ at x=0.01 is 0.75±0.16 at 916K (Fig.3d), a reduction by 40% compared to that in $C_{//}$.

The remarkable improvement of the electrical conductivity upon Zn substitution for In is due to the enhancement of free electron carriers, which is caused by the reduction of the number of interstitial In atoms (In_i) and Se vacancies (V_{se}) as well as new antisite defects Zn_{In}. Nonetheless, the number of In vacancy (V_{In}) remains almost unchanged, which has preserved its exchange between In cations and mobility (μ). The response of each species to the carrier concentration, n, is different. Some species acts as donors, while others act as acceptors. The detailed responses are estimated and summarized in Table 1. Taken together, the n-type carrier concentration (n) in the $In_{2-x}Zn_xSe_3$ system has a tendency to increase with Zn content increasing. In order to verify these estimations, we measured the Hall coefficients (R_h) and carrier concentrations (n) at RT (Table 2), and found that the n value in $C_{//}$ increases from 1.00×10^{23} (x = 0) to 7.64×10^{24} m^{-3} (x = 0.01), and that in $C\perp$ from 9.68×10^{22} (x = 0) to 6.73×10^{24} m^{-3} (x = 0.01). The carrier concentrations (n) in both $C_{//}$ and $C\perp$ are both about 2 orders of magnitude higher than those of pure α-In_2Se_3. The mobility (μ) has a similar compositional dependence to carrier concentration, but only about one order of magnitude higher. The samples at x=0.02 in both $C_{//}$ and $C\perp$ give lower n and μ values than those at x=0.01, which is probably due to the impurity of $Zn_{0.4}In_2Se_{3.4}$ precipitated. These data strongly verify the estimations shown in Table 1. The n value in pure α-In_2Se_3 is comparable to those in *ref.* 12(a),22, but the μ value is about 2~3 orders of magnitude smaller than the reported ones (1.90×10^{-3}m^{2}V^{-1}s^{-1}, *in-plane*)[12(a),22] and Li-intercalated In_2Se_3 single crystal (8.40×10^{-3}m^{2}V^{-1}s^{-1}).[22]

To better understand the effect of the structure on the lattice thermal conductivity, we specially analyzed the Raman spectra of three samples (x=0.005, 0.01 and pure α-In_2Se_3), which are shown in Fig.4. General features of the presented spectra bear resemblance to the results of Raman study performed by Lewandowska[23] and Kambas[24], as the structures in α-In_2Se_3 or its based alloys in our work are readily identified by the large peak at 106 cm^{-1}. This suggests that the molecular structures are rather similar and remain long-range ordering, even though the peak at 106 cm^{-1} becomes less pronounced upon the substitution of Zn for In. Furthermore, three modes at 180 cm^{-1}, 193 cm^{-1} and 203 cm^{-1} are combined in the α-In_2Se_3, but only two modes at 180 cm^{-1} and 203 cm^{-1} remain active in $In_{2-x}Zn_xSe_3$ (x=0.005, 0.01). The mode at 193 cm^{-1} seems to vanish completely, which implies that not only has the structure of Zn-substituted α-In_2Se_3 long-range ordering tendency, but it also gets more stabilized and has a short-range ordering tendency compared to Zn-free α-In_2Se_3, according to the suggestion from Zaretskaya et al.[25] These phenomena originate mainly from the reduction of interstitial In atoms (In_i) and Se vacancies (V_{Se}) upon the substitution of Zn for In, and they also explain the reduced lattice distortion and relatively high lattice κ_L values at high temperatures, although the new created antisite defect Zn_{In} can increase the lattice distortion to some extent. The Raman line at ~150 cm^{-1}, which presents in the Zn-substituted alloys, may be related to the presence of Zn-Se bonds in the structure.

Journal of Materials Chemistry C Accepted Manuscript

4. Conclusions

In this work, we have applied a non-equilibrium fabrication technology of materials (NEFT) to prepare the materials and present a promising layered structure TE material: a α-In_2Se_3-based solid solution upon substitution of Zn for In. This material gives the highest ZT value of 1.23(±0.22) at 916K through a successful manipulation of the lattice defects involving the reductions of the numbers of interstitial In atoms (In_i) and Se vacancies (V_{se}) as well as the creation of an antisite defect Zn_{In} as a donor. Such a manipulation directly leads to the enhancement of the carrier concentration and mobility and the remarkable improvement of electrical conductivity. However, the lattice thermal conductivity enhances to some extent, due to the fact that the structure tends to be ordering and more stabilized than that in the case of pure α-In_2Se_3.

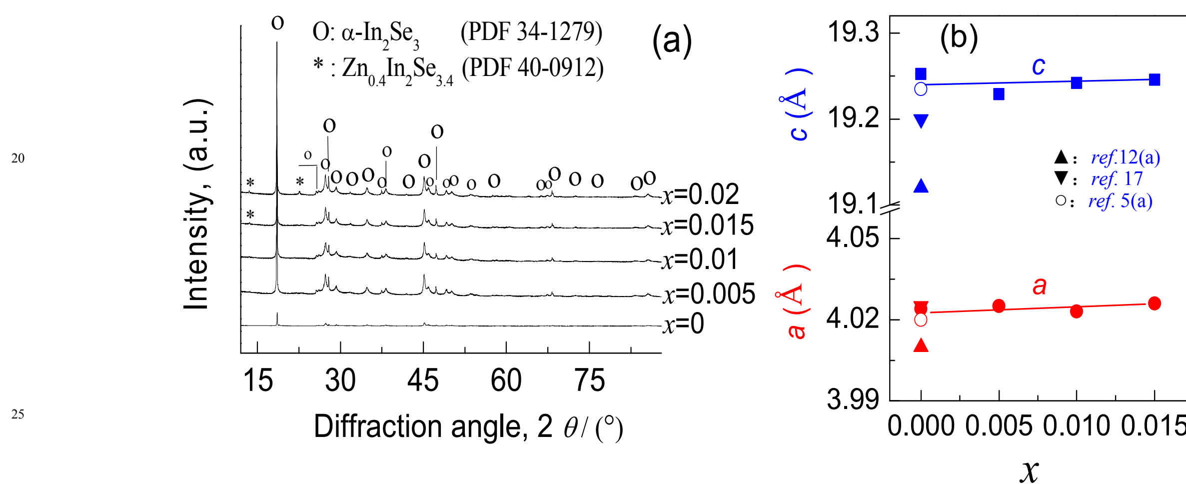

Fig. 1 (a) X-ray diffraction patterns of the $In_{2-x}Zn_xSe_3$ (x=0, 0.005, 0.01, 0.015, 0.02) powders, (b) Lattice constants a and c as a function of x value.

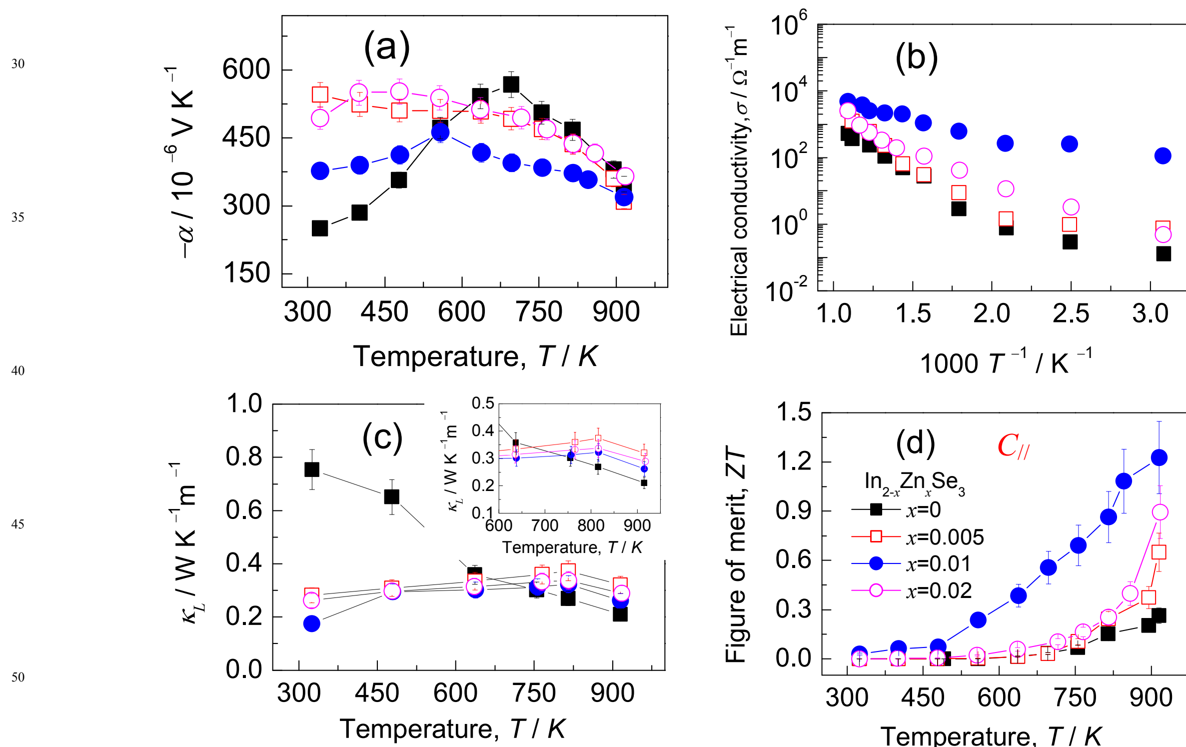

Fig. 2 Thermoelectric properties of $In_{2-x}Zn_xSe_3$ ((x=0, 0.005, 0.01, 0.02) samples along the pressing direction ($C_{//}$). (a) Seebeck coefficients (α), (b) Electrical conductivities (σ), (c) Lattice thermal conductivities (κ_L), an insert is a close-up view of κ_L, (d) Dimensionless figure of merit (ZT).

Journal of Materials Chemistry C Accepted Manuscript

This journal is © The Royal Society of Chemistry [year]

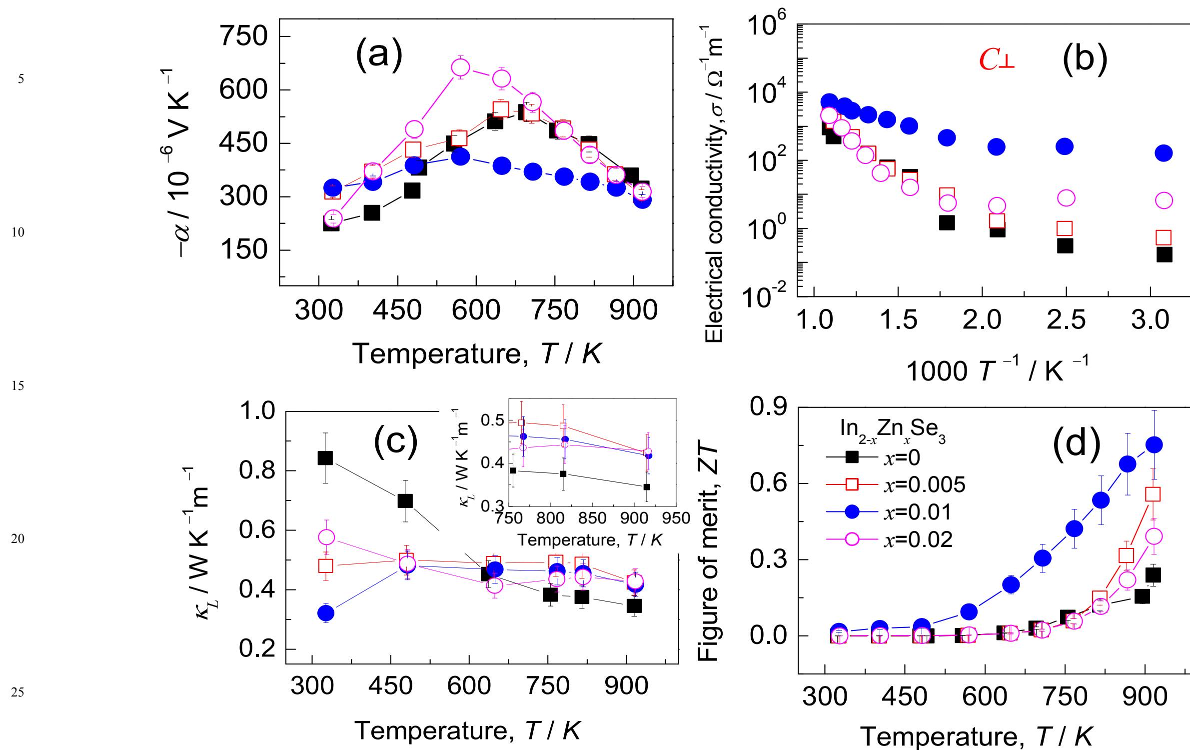

Fig. 3 Thermoelectric properties of $In_{2-x}Zn_xSe_3$ ((x=0, 0.005, 0.01, 0.02) samples perpendicular to the pressing direction ($C\perp$). (a) Seebeck coefficients (α), (b) Electrical conductivities (σ), (c) Lattice thermal conductivities (κ_L), an insert is a close-up view of κ_L, (d) Dimensionless figure of merit (ZT).

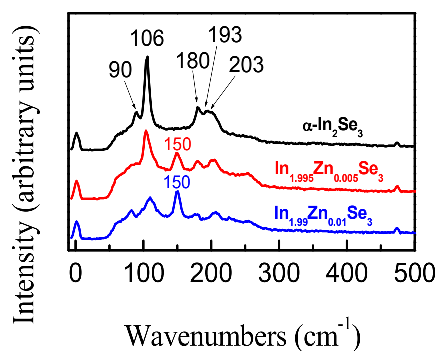

Fig. 4 Raman spectra of $In_{2-x}Zn_xSe_3$ ((x=0, 0.005, 0.01) samples.

Journal of Materials Chemistry C Accepted Manuscript

Table 1 Formations of cations (anions) and estimated changes of the carrier concentration (n) in different Zn-substituted $In_{2-x}Zn_xSe_3$

$In_{2-x}Zn_xSe_3$			
Possible formations of defects	Conducting type	Estimated carrier concentration (n)	Estimated change in n with x
Zn_{In}	donor	A certain quantity	Increase with x increasing
V_{In}	donor center	A large quantity	almost unchanged
In_i	donor upon interchange	A certain quantity	decrease with x increasing
V_{Se}	acceptor	A certain quantity	decrease with x increasing
VDW gap	-----	------	unchanged
Taken together, n–type carrier concentration (n) in $In_{2-x}Zn_xSe_3$			Increasing tendency

Table 2 Measured carrier concentrations n and mobility μ at RT of $In_{2-x}Zn_xSe_3$ (x=0, 0.005, 0.01, 0.02).

Samples	x	R_H (m^3/C)	Carrier concentration, n [$1/m^3$]	Mobility, μ [$m^2V^{-1}s^{-1}$]	σ [$\Omega^{-1}m^{-1}$]	Remarks
α-$In_{2-x}Zn_xSe_3$ ($C\perp$)	0	6.45×10^{-5}	9.68×10^{22}	1.10×10^{-5}	0.17	
	0.005	9.53×10^{-6}	6.56×10^{23}	6.86×10^{-6}	0.72	
	0.01	9.29×10^{-7}	6.73×10^{24}	1.51×10^{-4}	162.87	
	0.02	1.09×10^{-5}	5.72×10^{23}	5.08×10^{-5}	6.67	
α-$In_{2-x}Zn_xSe_3$ ($C_{//}$)	0	6.23×10^{-5}	1.00×10^{23}	7.93×10^{-6}	0.13	
	0.005	8.93×10^{-6}	7.00×10^{23}	6.71×10^{-6}	0.75	
	0.01	8.18×10^{-7}	7.64×10^{24}	9.22×10^{-5}	112.74	
	0.02	2.47×10^{-5}	2.53×10^{23}	1.19×10^{-5}	0.48	
$Li_{0.1}In_2Se_3$		0.42×10^{-6}	1.50×10^{25}	8.40×10^{-3}	2.00×10^{4}	from *ref.* 22
α-In_2Se_3		N/A	$5.00\sim7.22\times10^{22}$	1.90×10^{-3}	14.92	from *ref.*12(a),22

Journal of Materials Chemistry C Accepted Manuscript

This journal is © The Royal Society of Chemistry [year]

Acknowledgements

This work is supported by the National Natural Science Foundation of China (51171084, 50871056), Zhejiang Provincial Natural Science Foundation (LY14E010003), and Natural Science Foundation (2014A610016).

Notes and references

[a] School of Materials, Ningbo University of Technology, Ningbo 315016, China.
[b] Materials Science and Engineering College, China University of Mining and Technology, Xuzhou 221116, China
[c] Beijing Key Laboratory of Special Functional Materials and Films, School of Materials Science and Engineering, Beihang University, Beijing 100191, China
* Corresponding author, J.L.Cui, E-mail: cuijiaolin@163.com; Yuan Deng, E-mail: dengyuan@buaa.edu.cn

Electronic Supplementary Information (ESI) available: [Supporting Information is available from the RSC Online Library or from the author.]. See DOI: 10.1039/b000000x/

Journal of Materials Chemistry C Accepted Manuscript

REFERENCES

1 (a) K. Biswas, J. He, I. D. Blum, C.I.Wu, T. P. Hogan, D. N. Seidman, V. P. Dravid and M. G. Kanatzidis, *Nature*, 2012,**489**, 414; (b) B. Poudel, Q. Hao, Y. Ma, Y.g Lan, A. Minnich, B. Yu, X. Yan, D. Wang, A. Muto, D.Vashaee, X.Chen, J. Liu, M. S. Dresselhaus, G. Chen and Z. Ren, *Science*, 2008, **320**, 634; (c) W. Xie, J. He, H.J.Kang, X.Tang, S.Zhu, M. Laver, S.Wang, J.R.D.Copley, C.M. Brown, Q.Zhang and T. M. Tritt, *Nano Lett.*, 2010, **10,** 3283.

2 Y. Pei, X. Shi, A. LaLonde, H. Wang, L. Chen and G. J. Snyder, *Nature*, 2011, **473**, 66; (b) J.Rhyee, K.H.Lee, S.M.Lee, E.Cho, S.II Kim, E.Lee, Y.S.Kwon, J.H.Shim and G.Kotliar, *Nature*, 2009, **459**, 965; (c) J. P. Heremans, V. Jovovic, E. S. Toberer, A. Saramat, K. Kurosaki, A. Charoenphakdee, S. Yamanaka and G. J. Snyder, *Science*, 2008, **321**, 554; (d) W. Zhao, P. Wei, Q. Zhang, H. Peng, W. Zhu, D. Tang, J.Yu, H. Zhou, Z. Liu, X. Mu, D. He, J. Li, C. Wang, X.Tang and J.Yang, *Nat. Commun*., 2015, DOI: 10.1038, ncomms 7197

3 (a) S. Walia , R. Weber, S. Balendhran, D. Yao, J.T. Abrahamson, S. Zhuiykov, M. Bhaskaran, S. Sriram, M.S. Strano and K. Kalantar-zadeh. *Chem. Commun*., 2012, **48**, 7462; (b) S. Walia, S.Balendhran, P.Yi, D.Yao, S.Zhuiykov, M. Pannirselvam, R. Weber, M.S.Strano, M.Bhaskaran, S. Sriram and K. Kalantar-zadeh, *J. Phys. Chem.C* , 2013 , **117**, 9137; (c) S. Walia, R. Weber, S. Sriram, M. Bhaskaran, K. Latham, S. Zhuiykov and K. Kalantar-zadeh, *Energy Environ. Sci*., 2011, **4**, 3558; (d) S. Walia, R. Weber, K. Latham, P. Petersen, J.T. Abrahamson, M.S.Strano and K. Kalantar-zadeh, *Adv. Func. Mater*., 2011, **21**, 2072; (e) S. Shimizu, W.Choi, J.T. Abrahamson and M.SStrano, *phys. sta. sol.* b, 2011, **248**, 2445; (f) K.Y.Lee, H.Hwang, W.Choi, *ACS Appl.Mater.& Interfaces*,2014, **6**, 15575; (g) J.T. Abrahamson, B. Sempere , M.P. Walsh, J.M. Forman, F. Sen , S. Sen , S.G. Mahajan , G.L. Paulus , Q.H. Wang , W. Choi, M.S. Strano. *ACS Nano*, 2013, **7**, 6533.

4. Y.Watanabe, S.Kaneko, H.Kawazoe and M.Yamane, *Phys. Rev.* B, 1989,**40**, 3133.

5 (a) S. Popović, A. Tonejc, B. Gržeta-Plenković and R. Trojko, *J. Appl. Cryst.*, 1979,**12**,416; (b) S. Popović, B. Čelustka and D. Bidjin, *Phys. Stat. Sol.* a, 1971,**6**, 301; (c) D.Eddike, A.Ramdani, G.Brun, T.C.Tedenac, and B.Liautard, *Mater. Res. Bull.*, 1998, **33**, 519.

6 H. Suematsu and T. Okada, *J. Phys. Soc.Japan*, 1966, **21**, 1849.

7 (a) J. Cui, X.Zhang , Y. Deng, H. Fu, Y. M. Yan, Y. L. Gao and Y. Y. Li, *Scripta Mater.*, 2011,**64**, 510; (b) J. Cui, X.Liu, .Zhang, Y. Y. Li and Y. Deng, *J. Appl. Phys.*, 2011,**110**, 023708.

8 C. H. de Groot and J. S. Moodera, *J. Appl. Phys.*, 2001,**89**, 4336.

9 J.Ye, S.Soeda, Y.Nakamura and O.Nittono, *Jpn. J. Appl. Phys.*, 1998, **37**, 4264.

10 (a) B. Poudel, Q. Hao, Y. Ma, Y.C. Lan, A. Minnich, B. Yu, X. Yan, D.Z.Wang, A. Muto, D. Vashaee, X.Y.Chen, J.M.Liu, M.S. Dresselhaus, G. Chen and Z.F. Ren, *Science*, 2008,**320**, 634; (b) J. S. Rhyee1, K. H. Lee, S. M. Lee, E. Cho, S. II Kim, E. Lee, Y. S. Kwon, J. H. Shim and G. Kotliar, *Nature*, 2009,**459**, 965.

11 (a) M. Bredol and V. Leute, *J. Solid State Chem.*, 1985, **60**, 29. (b) H. v. Wensierski, D. Weitze and V Leute, *Solid State Ionics*, 1997, **101-103**, 479.

12 (a) C. Julien, E.Hatzikraniotis and K. Kambas, *Phys.Stat.Sol.* (a), 1986, **97**,579. (b) C.Julien, M.Eddrief, M. Balkanski, E.Hatzikraniotis and K. Kambas, *Phys. Stat. Sol.* (a), 1985,**88**, 687.

13 C.Julien and H.S.Mavi, *Mater. Sci.Eng.*(B), 1995, **30**, 27.

14 (a) M. Emziane, S. Marsillac and J.C. Bernède, *Mater. Chem. Phys.*, 2000,**62**, 84; (b) H. Ji, A. Reijnders, T. Liang, L.M. Schoop, K.S. Burch, N.P. Ong and R.J. Cava, *Mater. Res. Bull.*, 2013,**48**,2517; (c) J. Zhao and L.Yang, *J. Phys. Chem.* C, 2014,**118**, 5445; (e) G. Han, Z. Chen, J. Drennan and J. Zou, *Small*, 2004, 1-19, DOI: 10.1002/smll.201400104

15 (a) J.Yang, S. Chen, Z. Du, X. Liu and J.Cui, *Dalton Trans.*, 2014,**43**, 15228. (b) L.Wang, P. Ying, Y. Deng, H. Zhou, Z. Du and J. Cui, *RSC Adv.*, 2014,**4**, 33897.

16 J.F.Moulder and J. Chastain, *Handbook of X-ray hotoelectron Spectroscopy: A Reference Book of Standard Spectra for* 35 *Identification and Interpretation of XPS Data*; Perkin–Elmer Corporation: Physical Electronics Division, Eden Prairie, Minnesota, p.261.1992.

17 H.Miyazawa and S. Sugaike, *J. Phys. Soc. Japan*, 1957,**12**, 312.

18 G.D. Mahan and M.Bartkowiak, *Appl. Phys. Lett.*, 1999,**74**, 953.

19 (a) R. Liu, H. Xi, H. Liu, X.Shi, W.Zhang and L.Chen, *Chem.Commun.*, 2012,**48**,3818; (b) T.Plirdpring, K.Kurosaki, A.Kosuga, T.Day, S.Firdosy, V.Ravi, G.J.Snyder A.Harnwunggmoung, T.Sugahara, Y.Ohishi, H.Mut and S.Yamanaka, *Adv. Mater.*, 2012,**24**, 3622; (c) J. Zhang, R. Liu, N. Cheng, Y. Zhang , J. Yang, C. Uher , X. Shi , L. Chen and W. Zhang, *Adv. Mater.*, 2014,**26**, 3848.

This journal is © The Royal Society of Chemistry [year]

Journal of Materials Chemistry C Accepted Manuscript

20 Y. Luo, J. Yang, G. Li , M. Liu, Y. Xiao, L. Fu, W. Li, P. Zhu, J. Peng, S. Gao and J. Zhang, *Adv. Energy Mater*. 2014,**4**, 1300599.
21 (a) Z. Lin , L. Chen , L. Wang , J. Zhao and L. Wu, *Adv. Mater.*, 2013, **25**, 4800; (b) J.S. Rhyee, K. Ahn, K.H. Lee, H. S. Ji and J.H.Shim, *Adv. Mater.*, 2011,**23**, 2191.
22 C. Julien and M. Balkanski, *Mater. Sci. Eng.* B, 1996,**38**, 1.
5 23 R. Lewandowska, R. Bacewicz, J. Filipowicz and W. Paszkowicz, *Mater. Res. Bull.*, 2001,**36**, 2577.
24 K. Kambas, C. Julien, M. Jouanne, A. Likforman and M. Guittard, *Phys.Stat.Sol.* (b), 1984,**124**, K105.
25 E.P. Zaretskaya, V.F. Gremenok, V. Riede, W. Schmitz, K. Bente, V.B. Zalesski and O.V. Ermakov, *J. Phys. Chem. Solids*, 2003,**64**, 1989.

Journal of Materials Chemistry C Accepted Manuscript